PROTEINS: Structure, Function, and Genetics 11:184–204 (1991)

A 175-psec Molecular Dynamics Simulation of Camphor-Bound Cytochrome P-450$_{cam}$

Mark D. Paulsen and Rick L. Ornstein
Molecular Science Research Center, Pacific Northwest Laboratory, Richland, Washington 99352

ABSTRACT **The structure and internal motions of cytochrome P-450$_{cam}$, a monooxygenase heme enzyme with 414 amino acid residues, with camphor bound at the active site have been evaluated on the basis of a 175-psec molecular dynamics simulation carried out at 300 K. All hydrogen atoms were explicitly modeled, and 204 crystallographic waters were included in the simulation. Based on an analysis of the time course of the trajectory versus potential energy, root mean square deviation, radius of gyration, and hydrogen bonding, the simulation was judged to be stable and representative of the average experimental structure. The averaged structural properties of the enzyme were evaluated from the final 135 psec of the simulation. The average atomic displacement from the X-ray structure was 1.39 Å for all heavy atoms and 1.17 Å for just C-α atoms. The average root-mean- square (rms) fluctuations of all heavy atoms and backbone atoms were 0.42 and 0.37 Å, respectively. The computed rms fluctuations were in reasonable agreement with the experimentally determined temperature factors. All 13 segments of α-helix and 5 segments of β-sheet were well preserved with the exception of the N-terminal half of helix F which alternated between an α-helix and a 3_{10}-helix. In addition there were in general only small variations in the relative orientation of adjacent α-helices. The rms fluctuations of the backbone dihedral angles in the secondary structure elements were almost uniformly smaller, with the fluctuation in α-helices and β-sheets, 31 and 10% less, respectively, than those in nonsecondary structure regions. The reported crystal structure contains kinks in both helices C and I. In the simulation, both of these regions showed high mobility and large deviations from their starting positions. Since the kink in the I helix is at the oxygen binding site, these motions may have mechanistic implications.**

Key words: heme enzyme, *Pseudomonas putida*, conformational flexibility, protein dynamics

INTRODUCTION

The internal motions of proteins are critical to their proper functioning. In particular, protein–protein recognition or substrate binding to the active site of an enzyme may involve a wide variety of conformational changes including local side chain motions, secondary structure movements, loop closings, and hinge bendings. Such dynamic processes which occur on a wide variety of time scales will generally not be apparent from structural data obtained from X-ray crystallography or NMR studies which mostly give time-averaged information about only the most highly populated states.

One method used to probe these types of structural fluctations of proteins is molecular dynamics simulations.[1,2] Such simulations can be used to probe both equilibrium properties and time-dependent phenomena. Simulations of enzymes such as carboxypeptidase A[3], ribonuclease T_1,[4] and triose phosphate isomerase[5] have provided insight into enzyme motions which may play a key role in the enzyme mechanism.

The cytochromes P-450 are a ubiquitous superfamily of heme-containing monooxygenases found in both prokaryotes and eukaryotes. These enzymes function in a wide number of biochemical oxidation reactions including metabolism of xenobiotic compounds, steroid hormone biosynthesis, and activation of polycyclic aromatic hydrocarbons to mutagenic and carcinogenic compounds.[6] The importance of the cytochromes P-450 in detoxification, drug metabolism, and activation of potential carcinogens has made this enzyme superfamily the subject of intense scientific scrutiny. One of the most well-studied forms of cytochrome P-450 is the camphor hydroxylase (P-450$_{cam}$) from *Pseudomonas putida*.[7] It is also the only cytochrome P-450 for which a three-dimensional structure has been determined. Structures have been determined for both the substrate-free and substrate-bound forms.[8,9] In addition, structures have also been determined for P-450$_{cam}$ complexed with four different inhibitors,[10] with the alternative substrates norcamphor and adamantane, both of which can be hydroxylated by cytochrome P-450$_{cam}$,[11] and as a ternary complex with

Accepted for publication March 29, 1991.
Address reprint requests to Dr. Rick L. Ornstein, Molecular Science Research Center, Pacific Northwest Laboratory, P.O. Box 999, Richland, WA 99352.

both camphor and carbon monoxide bound at the active site.[12]

An interesting feature of the cytochrome P-450–camphor complex is that the active site is well sequestered in the enzyme with essentially no solvent exposure and no obvious route from the molecular surface to the active site.[9] The crystallographic study of the substrate-free form of the enzyme reveals no significant increase in the solvent exposure of the active site relative to the camphor-bound form.[8] The sequestering of the heme moiety is a common feature of the heme enzymes for which structures have been determined and is presumably necessary to protect the highly reactive radical and iron–oxygen intermediates. Thus conformational flexibility and dynamic fluctuations are necessary for substrate binding and product release to occur. Such "gate-opening" motions have been observed for ligand binding to myoglobin and other proteins.[2] For the myoglobin case, the substrate is a diatomic molecule. In contrast, camphor contains 27 atoms; hence the conformational mobility and dynamic motions necessary for substrate binding and product release must be significantly greater than seen for myoglobin. One objective in our investigation is to identify those structural fluctuations which may play a key role in allowing access to the active site of cytochrome P-450$_{cam}$. In this paper, we present the results of a 175-psec molecular dynamics simulation of cytochrome P-450$_{cam}$. In the simulation, interesting motions were seen in the region containing the F and G helicies, which sit directly above the active site. In addition unusual mobility was also seen in the region surrounding Thr-252. Since this residue is at the oxygen-binding site, the observed motions may have mechanistic implications.

METHODS

The coordinates of the reported X-ray structure of cytochrome P-450$_{cam}$ at 1.63 Å resolution,[9] obtained from the Brookhaven Protein Data Bank,[13] served as the initial molecular model for the molecular dynamics (MD) calculations. The system simulated was comprised of 3,324 heavy atoms encompassing amino acid residues 10 through 414 of the protein plus the heme moiety and the bound camphor at the active site. In addition, 204 crystallographic waters were included in the simulation. All of the hydrogen atoms were explicitly modeled bringing the total number of atoms in the system to 7,083. Use of the published consistent valence force field united atom parameters can result in a significantly larger drift away from the crystal coordinates and an overall compaction of the protein.[14] The coordinates of the added hydrogens were generated according to idealized bond lengths and valence angles using the MOLEDT software package from Biosym Technologies.

The MD simulation was performed using the Discover simulation software package (version 2.41) from Biosym Technologies on a Cray XMP. With the exception of the heme group, the parameters used in the force field were those of the standard Discover library.[15,16] The default Discover model was used for the explicit waters. No cross-terms were used in the energy expression, and a simple harmonic potential was chosen for the bond-stretching terms. The bond, valence angle, and torsional angle terms unique to the heme group were based on the values determined by Giammona.[17] The iron atom in the heme group was assumed to be covalently linked to the sulfur atom of the axial cysteine residue. Values of A_{ii} = 3,355,443 kcal-Å^{12}/mol and B_{ii} = 16,038.4 kcal-Å^{6}/mol for the iron atom were used in the Lennard–Jones interaction term. Because there were no unique bonds, valence angles, or torsion angles in the camphor molecule, the forcefield parameters were taken from the standard forcefield library. The partial atomic charges used for the camphor and the heme group are given in Table I. To compensate for the absence of the shielding influence of the bulk solvent, charged amino acid side chains and terminal residues were made net-neutral and a linear distance-dependent dielectric (equal to the interatomic separation) was used.

Initially, the X-ray structure was subjected to energy minimization using the method of steepest descents for 500 iterations with all heavy atoms fixed to remove any artifacts introduced by the addition of explicit hydrogen atoms. The structure was further minimized with only the protein heavy atoms positions fixed for 500 iterations to allow the waters to relax. Following this, the entire system was subjected to minimization using the conjugate gradients

TABLE I. Partial Atomic Charges Used for the Heme Group

Atom	Charge
SG	−0.100
FE	1.280
NA,NB,NC,ND	−0.500
C1A,C1B,C1C,C1D	0.100
C2A,C2B,C2C,C2D	−0.050
C3A,C3B,C3C,C3D	−0.050
C4A,C4B,C4C,C4D	0.100
CMA,CMB,CMC,CMD	−0.250
CAA,CBA,CBB,CBC,CAD,CBD	−0.150
CAC,CAB	−0.050
CGA,CGD	0.450
O2A,O2D	−0.505
O1A,O1D	−0.505
CHA,CHB,CHC,CHD	−0.100
Partial Atomic Charges Used for Camphor	
Atom	Charge
C1,C4,C7	−0.100
C2	0.380
O	−0.380
C3,C5,C6	−0.200
C8,C9,C10	−0.300

method for 5,000 steps to relax any remaining hot spots before beginning the MD simulation. The resulting structure had an rms deviation away from the crystal coordinates of 0.83 Å.

The molecular dynamics integrations were done using a leapfrog algorithm with a time step of 1.0 fsec. The simulation was carried out at a constant temperature of 300 K by weakly coupling the system to a thermal bath whereby the atomic velocities were rescaled at each time step.[18] The time constant used to couple the system to the thermal bath was 0.1 psec. Nonbonded interactions were evaluted with a group-based switching function between 9.5 and 11.5 Å, and the nonbonded pair list was updated every 20 time steps. The initial velocities were obtained from a Maxwellian distribution at 50 K. The system was then slowly warmed to 300 K over the course of 10 psec. After the warming period, the simulation was continued for an additional 165 psec.

RESULTS AND DISCUSSION

In the following sections we describe the analysis of the molecular dynamics simulation of the camphor-bound cytochrome P-450$_{cam}$ complex. We focus first on the evolution of several system variables during the time course of the simulation. These variables can be used to judge the stability of the trajectory. The output of the simulation in the form of cartesian coordinates of each atom in the system as a function of the time course of the simulation is then analyzed in terms of the time-averaged structure, the hydrogen bonding pattern, rms deviations of individual secondary structure elements, and atomic fluctuations.

Analysis of the Time Course of the Simulation

In order to assess the stability of the trajectory, several system properties including the potential energy, the radius of gyration, the rms deviation in position away from the X-ray coordinates, and the hydrogen bonding pattern were monitored as a function of the time course of the simulation. The variation in potential energy as a function of time is shown in Figure 1A. Initially, the energy was quite low, which reflects the fact that the starting structure was thoroughly minimized. After the gradual rise over the first 10 psec during the warmup phase of the simulation, the energy leveled off and then remained fairly constant for the duration of the simulation. The drift in the energy over the final 100 psec is 0.013%/psec.

In Figure 1B, the variation in the radius of gyration of cytochrome P-450$_{cam}$ is plotted as a function of time. After increasing by 1.5% during the equilibration period, the radius of gyration was also stable during the remainder of the simulation. The slight increase in the radius of gyration during the early portion of this simulation contrasts the result seen when no crystallographic waters are included in the simulation (data not shown); in which case, the radius decreased by 2.5%. The slight increase also contrasts the small decreases in the radius of gyration seen for carboxypeptidase A[3] and lysozyme.[19] The carboxypeptidase simulation was performed with 25 structural water molecules; while in the lysozyme simulation, 53 structural water molecules were modeled. For the present simulation, 204 waters were included. Perhaps more importantly, both the lysozyme and carboxypeptidase simulations were done using the united-atom approximation for nonpolar hydrogens, whereas the present simulation was done using an all-atom model. The average value of the radius of gyration during the simulation was 21.67 ± 0.08 Å, which is slightly less than the experimentally measured value of 23.9 Å obtained from small-angle X-ray scattering studies.[20] This difference could be due, at least in part, to a layer of bound water on the surface of the protein which may contribute to the experimentally measured value but was not included in our calculation of the radius of gyration. The radius of gyration calculated from the crystal coordinates is virtually identical to that determined for the initial energy minimized structure.

The rms deviations in the position of all nonhydrogen atoms, of just the backbone atoms, and of just the backbone atoms in secondary structure elements away from the crystal coordinates are shown as a function of time in Figure 1C. The rms deviation for the heavy atoms was 0.83 Å for the minimized starting structure and rose to approximately 1.5 Å during the warmup phase of the simulation. For just the backbone heavy atoms, the rms deviation after energy minimization was 0.66 Å and rose to 1.2 Å during the equilibration phase. Over the final 125 psec, the average rms deviation for the heavy atoms is 1.91 Å, while the average deviation for the backbone atoms is 1.58 Å. If just the residues in secondary structure elements are considered, the average rms deviation of the final 125 psec is only 1.23 Å.

In Figure 2A, the number of backbone–backbone hydrogen bonds is plotted as a function of the time course of the simulation. In the initial energy-minimized structure, the total number of backbone–backbone hydrogen bonds was 266. This number was determined using both distance and angle criteria. All acceptor atom–hydrogen distances of less than 2.5 Å were counted as hydrogen bonds if the hydrogen bond angle was 180 ± 35°. These fairly generous criteria will probably include a number of weaker hydrogen bonds. During the first few picoseconds of the trajectory, the number of hydrogen bonds decreased substantially as the added thermal energy broke some of the weaker hydrogen bonds. Over the final 165 psec of the simulation, there was an average of 179 backbone–backbone hydrogen bonds. Also shown in Figure 2A is the number of hydrogen bonds in each archived structure that

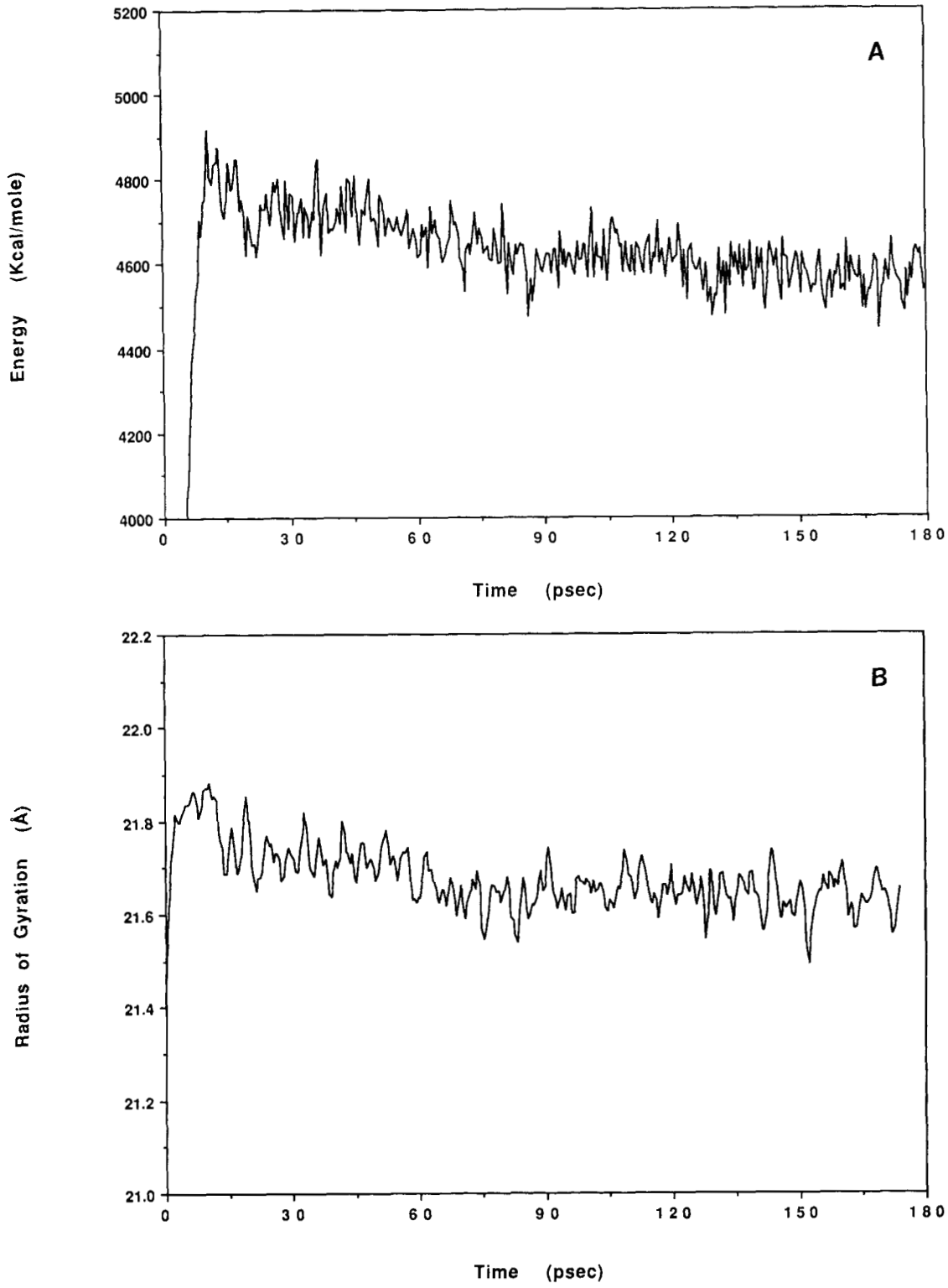

Fig. 1. Time course of the molecular dynamics simulation: **(A)** The total potential energy of the system (enzyme, camphor, and explicit waters); **(B)** the calculated radius of gyration of cytochrome P-450$_{cam}$; **(C)** the root mean square deviation in position away from the crystallographic coordinates. The solid line is the rms deviation of all protein heavy atoms, the dotted line is the rms deviation of just the backbone atoms, and the dashed line is the rms deviation of backbone atoms in the secondary structure domains. Figure 1 **C** appears on page 188.

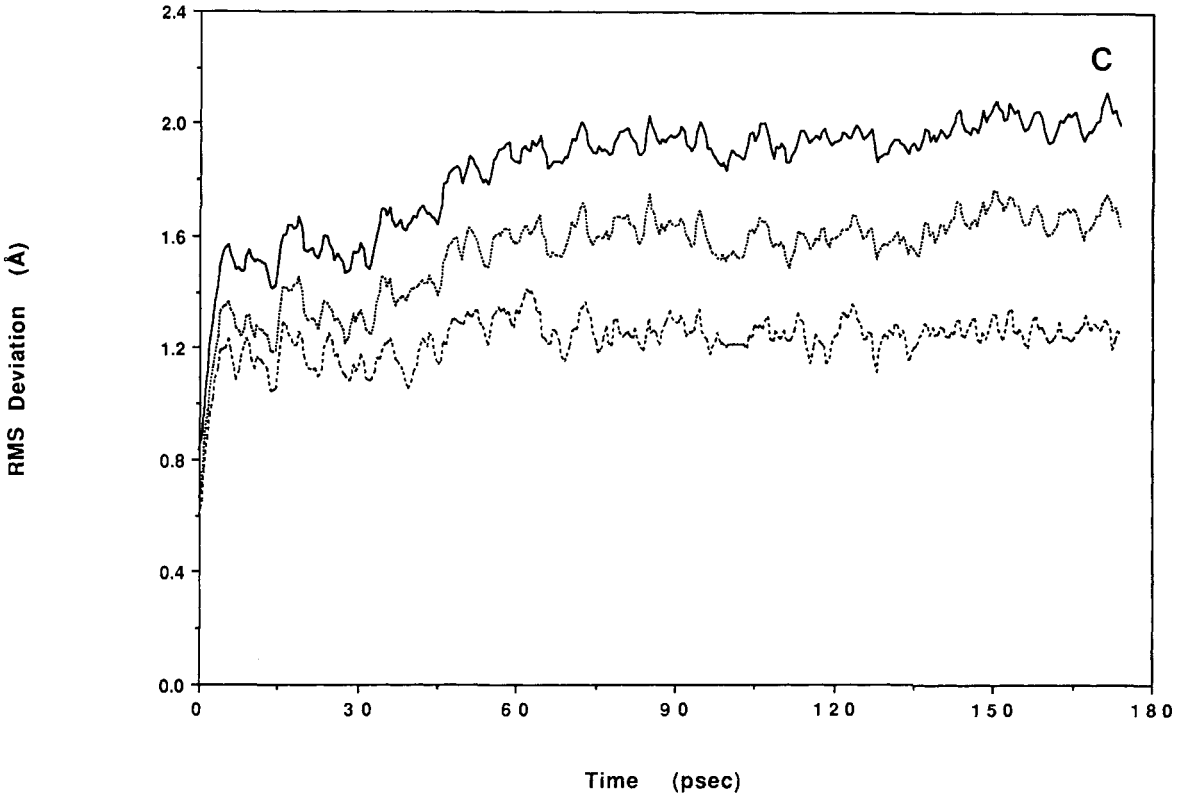

Fig. 1C. Legend appears on page 187.

were also present in the initial minimized structure, i.e., the same atoms on the same residues were involved as donor and acceptor. We refer to these hydrogen bonds as conserved ones. Again, after an initial drop, the number reached a stable equilibrium. The average number of conserved backbone–backbone hydrogen bonds over the last 165 psec was 137, only 52% of the starting value of 266 and 76% of the average number of total backbone–backbone hydrogen bonds. It is interesting to note that a significant amount of hydrogen bond exchange occurs during the simulation.

A similar plot is shown in Figure 2B for hydrogen bonds involving side chains. In contrast to the backbone hydrogen bonds, there was almost no decrease in the total number of side chain hydrogen bonds during the warmup phase of the simulation. The average number of sidechain hydrogen bonds over the final 165 psec of the simulation is 53 compared with an initial value of 61. Similar to the case of the backbone hydrogen bonds, the average number of conserved side chain hydrogen bonds is significantly lower than the average total number of side chain hydrogen bonds. The average number of conserved side chain hydrogen bonds per structure is 29, slightly more than half of the average total number of side chain hydrogen bonds. Based on the data presented in Figures 1 and 2, we chose to use the last 135 psec of the simulation to calculate the average properties of substrate-bound P-450$_{cam}$.

Analysis of the Average Properties of the Trajectory

Before discussing the time-averaged simulated structure as compared with the X-ray crystal structure, it will be useful to review the X-ray structure of cytochrome P-450$_{cam}$ as determined by Poulos and co-workers.[9] The basic shape of the enzyme, shown in Figure 3A and B, is a trigonal prism divided into a helix-rich domain, above the heme group in the view presented in Figure 3A, and a helix-poor domain. The enzyme consists of 18 secondary structure elements, 13 α-helices which Poulos and coworkers label A through L, and 5 β-sheets labeled β-1 through β-5. The heme group at the active site is sandwiched between helices I and L with the sulfur atom on Cys-357 serving as one axial ligand for the heme iron. The heme group and the camphor at the active site are surrounded by protein with virtually no solvent accessibility.

The atomic coordinates of every atom in the simulation over the final 135 psec of the trajectory were used to determine a time-averaged structure for cytochrome P-450$_{cam}$. The rms difference in the coordinates of all the heavy atoms between the X-ray structure and the time-averaged structure is 1.39 Å.

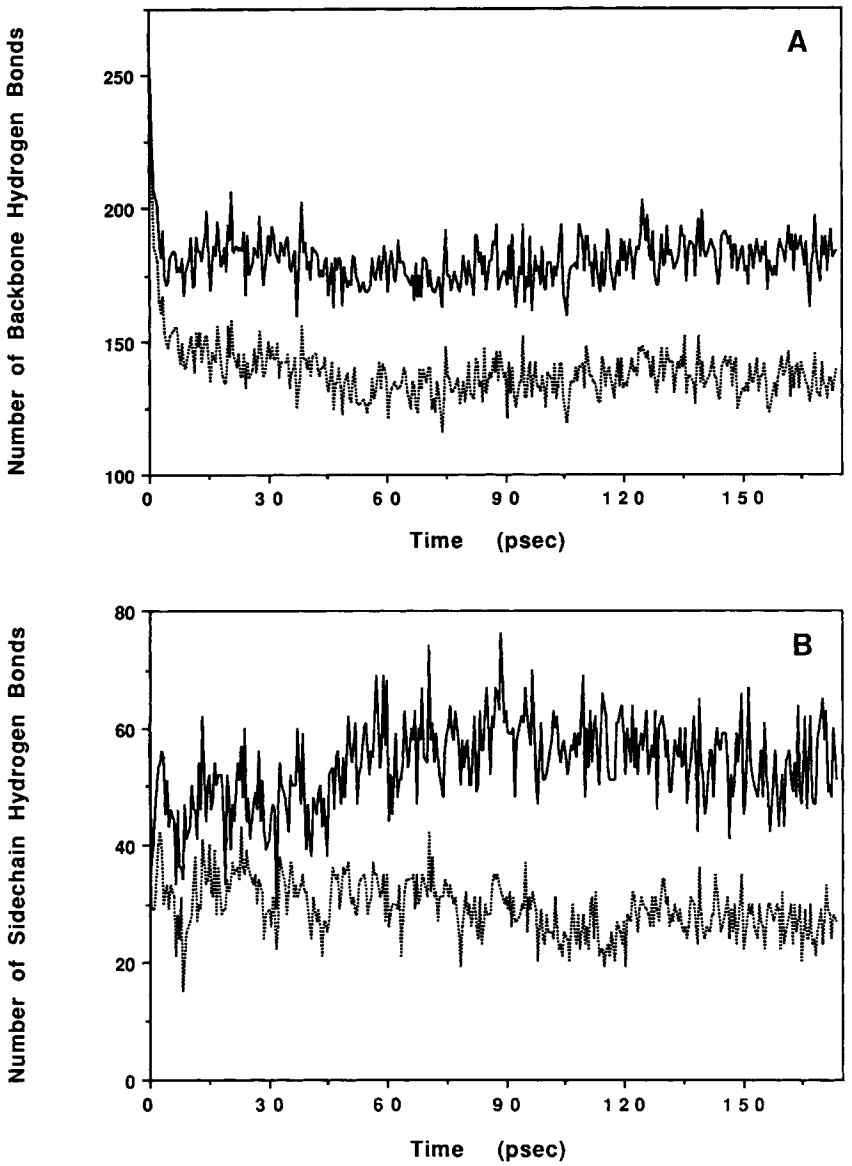

Fig. 2. Number of total (solid line) and conserved (dotted line) hydrogen bonds found in cytochrome P-450$_{cam}$ plotted as a function of time: **(A)** backbone–backbone hydrogen bonds and **(B)** side chain hydrogen bonds.

For just the C-α atoms, the rms difference is 1.17 Å. The heavy atom rms difference can be compared with values of 2.2 Å for lysozyme,[19] 1.19 Å for bovine pancreatic trypsin inhibitor,[21] 1.82 Å for the C-terminal fragment of the L7/L12 ribosomal protein,[22] and 2.49 Å for carboxypeptidase.[3] The corresponding values for just the C-α atoms are 1.5 Å for lysozyme, 0.82 Å for bovine pancreatic trypsin inhibitor, 1.07 Å for L7/L12, and 1.79 Å for carboxypeptidase.

In Figure 4, the displacement between the C-α atoms in the crystal structure and the time-averaged structure is plotted as a function of residue number. As can be clearly seen, the discrepancies between the time-averaged structure and the X-ray structure are not distributed uniformly. The average displacement for residues in the various secondary structure elements is 0.89 Å; while for the molecule as a whole, it is 1.14 Å. The largest movement occurred in the various turn regions. Large displacements are especially evident in the turns between helices E and F, F and G, and H and I. In addition, the irregular surface loop from residue 337 to residue 347 shows significant differences between the starting structure and the time-averaged structure. The large deviations in these regions may indicate that the crystal conformation is strongly influenced by intermolecular contacts and lattice packing

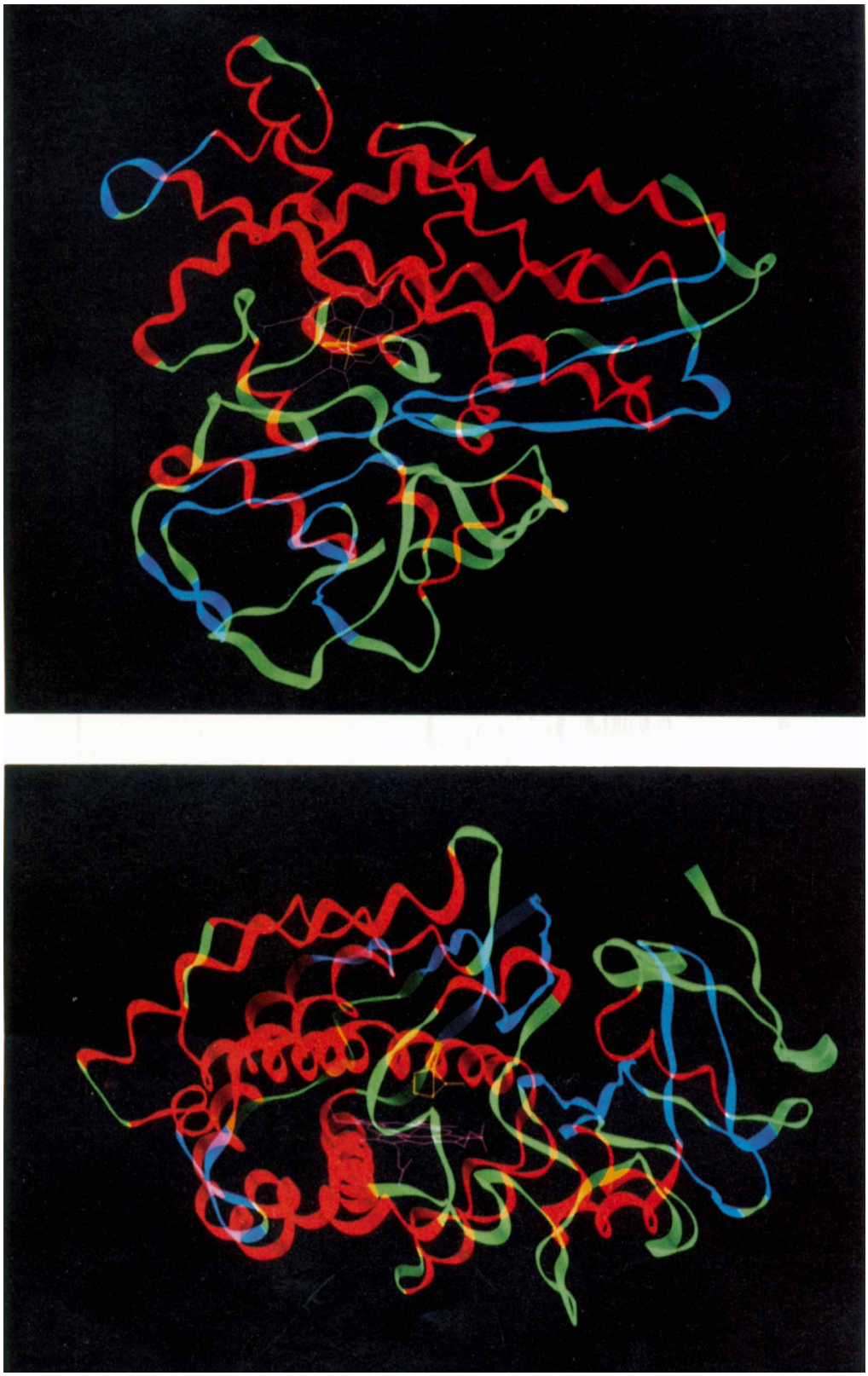

Fig. 3. A view down the heme normal of a ribbon drawing of the backbone atoms of cytochrome P-450$_{cam}$. The 13 α-helices are colored red and the 5 β-sheets are blue. Those residues not part of a helix or sheet are green. The bound camphor is in yellow and the heme group at the active site is magenta. (In those regions where residues of different color overlapped, the color blended.)

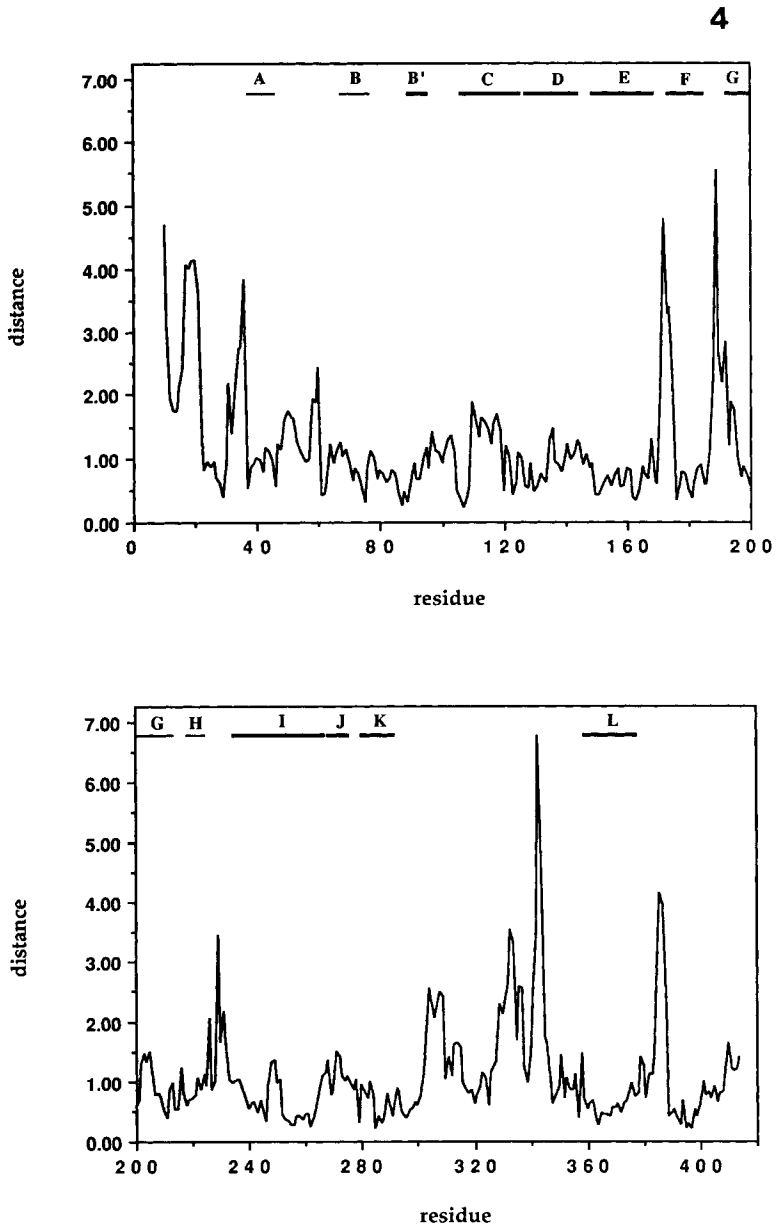

Fig. 4. Difference in Ångstroms between the X-ray and molecular dynamics average coordinates of the 405 C-α atoms of cytrochrome P-450$_{cam}$ plotted versus the residue number. The 13 segments of α-helix are labeled by horizontal bars.

forces which will not be present in a simulation of an isolated protein. In contrast, with the exception of β-4, the C-α positions of the 18 secondary structure domains generally show small deviations between the starting structure and the time-averaged structure.

Figure 5 shows a plot of the difference in backbone dihedral angles Φ and Ψ in the X-ray crystal structure and the average molecular dynamics structure. Some regions of the enzyme exhibited quite large differences in the Φ and Ψ angles in each of the structures. For instance, the turns between helices D, E, F, G, H, and I all have some residues showing changes in backbone dihedral angles of 50° to 100° or more from their initial values. The irregular surface loop leading into Cys-357, which is the axial ligand for the heme group, also shows significant deviations in Φ and Ψ. However, in these regions there is usually a pattern of correlated positive and negative values of ΔΦ and ΔΨ in adjacent residues. Such correlated changes have been observed in molecular dynamics simulations of other proteins and have been shown to preserve the general direction of the backbone.[23] As an example of the effect of correlated

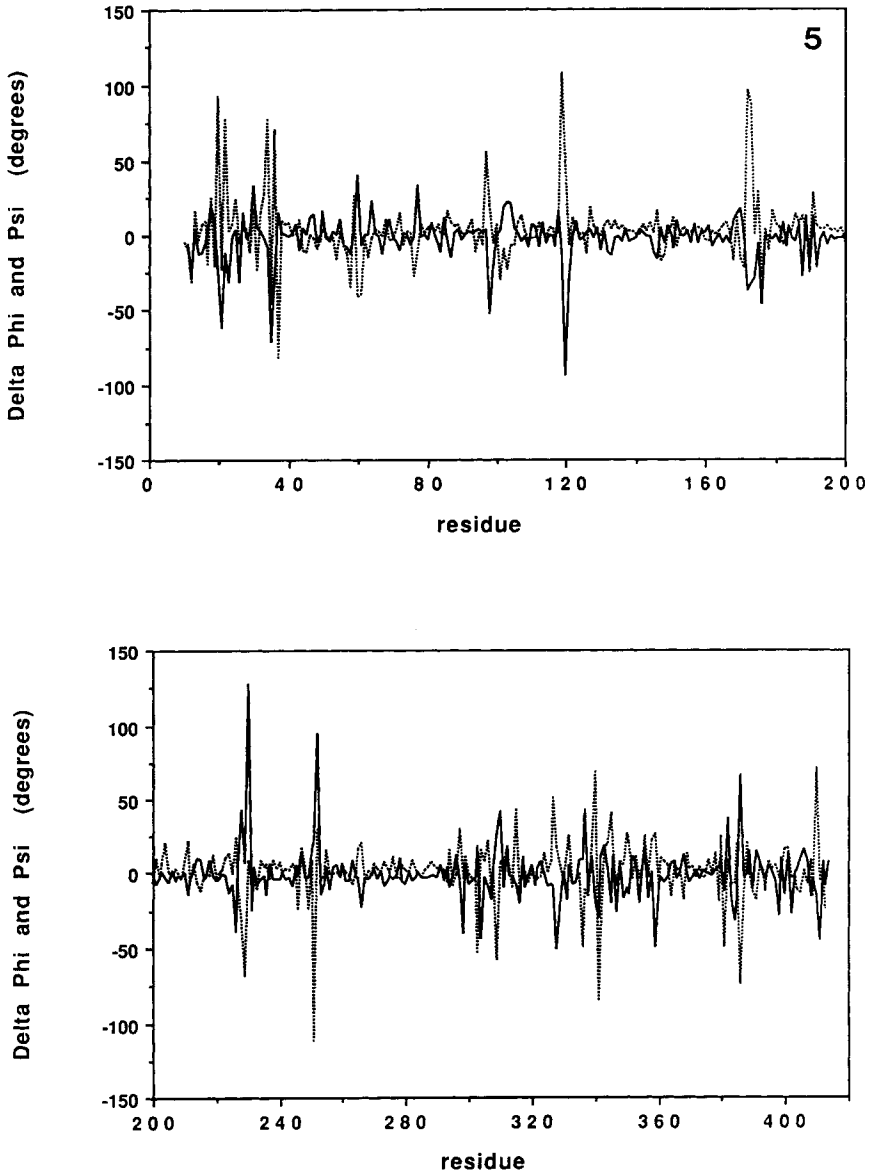

Fig. 5. Difference in degrees between the values of the backbone dihedral angles Φ (solid line) and Ψ (dotted line) in the average structure and in the initial structure plotted versus the residue number.

changes on the general direction of the backbone trace, we show in Figure 6 superimposed plots of the initial and average structure of the turn regions between helices F and G and between helices G and H. Both of these turns exhibited large changes in some Φ and Ψ angles, but the effects of these changes are fairly local and do not alter the basic direction of the two helices on either side of the turns. The turn between helices B′ and C also show some large differences in backbone dihedral angles. In addition the last two residues of helix B′, Ala-95 and Tyr-96, have undergone significant changes in Φ and Ψ. This shift is interesting because the X-ray analysis suggested that a cation may be coordinated to the carbonyl oxygen of Tyr 96 as well as three nearby carbonyl oxygens and two water molecules stabilizing an otherwise unfavorable polypeptide conformation.[9] Since no cations were included in the simulation, the observed shift in dihedral angles is consistent with the hypothesis that the cation is necessary to stabilize the protein backbone. It would be interesting to see if the replacement of that particular water molecule in the simulation with an appropriate cation would result in significantly smaller changes in the backbone dihedral angles in this region.

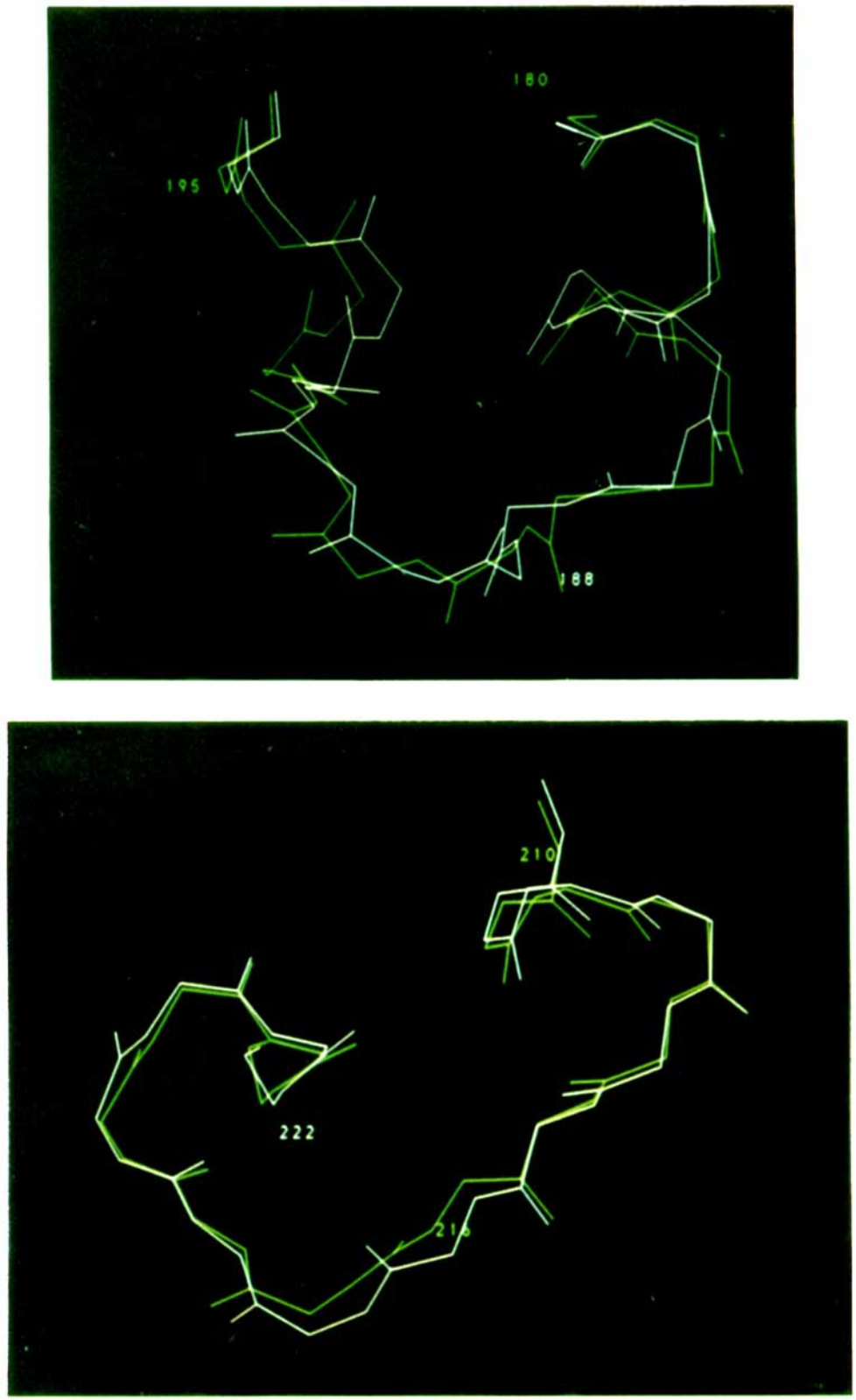

Fig. 6. Superimposed plots of the backbone atoms of the turns between **(Top)** helices F and G and **(Bottom)** between helices G and H both of which exhibited large correlated changes in Φ and Ψ. In both figures, the starting crystal structure is in green and the time-averaged structure is in white.

For the residues defining the secondary structure elements, the differences in the backbone dihedral angles between the time-averaged structure and the starting X-ray structure were generally much smaller than for the protein as a whole. The average change in Φ and Ψ was 8.23° for those residues that are part of α-helices as compared with an average difference of 13.15° for all residues. There were only two real exceptions to this pattern. One of these involves correlated changes in backbone dihedral angles in the middle of the distal helix I, at residues Asp-251 and Thr-252, where the backbone dihedral angles in the time-averaged structure have changed from their starting values by around 65°. In the crystal structure these two residues are distorted away from a helical conformation and form the presumed oxygen binding pocket.[9,12] Mutation of Thr-252 causes a significant increase in the decoupling of electron transfer from the hydroxylation reaction.[24,25] However, in the time averaged structure, both residues have adopted conformations much closer to a normal α-helix. The Asp-251Φ and Ψ dihedral angles change from −83.5° and 77.1° in the minimized starting structure to −62.3° and −34.8°, respectively, in the time-averaged simulation. Likewise, the Thr-252 dihedral angles shift from −151.9° and −75.7° to −57.5° and −46.2°, respectively. This shift in conformation occurred at 12 psec into the simulation, shortly after the end of the warmup period, and the residues retained their new conformation for the remainder of the simulation.

This observation suggests that in the absence of an axial ligand, the kinked conformation is not the most stable conformation. This is difficult to reconcile with the crystallographic data in which no axial ligand was present and yet the kinked conformation was clearly the most populated. It is possible that crystal lattice forces were responsible for promoting the kink, but this would be somewhat surprising considering that it occurs in a deeply buried portion of the enzyme. It is also possible that the motion observed in the simulation is an artifact of the approximations made in the calculation. However, considering the small changes noted in the average structure for most residues in the regions of secondary structure, it is difficult to identify what approximation in the forcefield or calculation might be responsible for the observed change in conformation for this particular region. In addition the current simulation cannot answer the question of whether or not the presence of an axial ligand would stabilize the kink.

The other region of large changes in Φ and Ψ, within a secondary structure unit, occurs at residues Val-119 and Gly-120 in the middle of helix C. In both residues, the backbone dihedral angles show changes of over 100°. The transition of the backbone dihedral angles occurred very early in the warmup period of the simulation. Although the two residues are in the middle of a long stretch of α-helix, neither residue has backbone dihedral angles, in the crystal structure, characteristic of α-helical residues. In contrast to the case of the I helix, the shifts in Φ and Ψ for residues 119 and 120 do not result in a structure which is closer to the ideal α-helix. In the crystal structure, Val-119 is in close contact with one of the two vinyl groups on the heme. The conformational change allows for a slightly longer distance between the heme vinyl group and Val-119. In the crystal structure of the ternary P-450–camphor–CO complex it was noted that this vinyl group was rotated by about 140° from its position in the binary complex.[12] In our simulation, the conformational changes in residues 119 and 120 are not correlated with any rotation of the vinyl group, which retains its original conformation throughout the simulation.

As might be expected, there was much less variation in the Ω backbone dihedral angles than in the Φ and Ψ angles. None of the 3 *cis*-prolines nor any of the 27 *trans*-prolines underwent a *cis-trans* isomerization during the simulation. This is in constrast with the recent simulations of carboxypeptidase A[3] and the L7/L12 ribosomal protein[22] where *cis-trans* isomerizations were observed during the course of those trajectories. In addition, no Ω angle in the time-averaged structure varied from its initial value by more than 10%. In view of the high energy barrier to isomerization, such transitions on the subnanosecond time scale are not expected to occur.

Hydrogen Bonding Analysis

The hydrogen bonding pattern in cytochrome P-450_{cam} is essential for maintaining the folded structure. This pattern has been analyzed in more detail to compare the bonding pattern in the average structure with the crystal structure and to determine which hydrogen bonds were the longest lived. Using both a distance and an angle criteria, it was determined that 70% of the hydrogen bonds found in the crystal structure were also present in the time-averaged structure. This percentage can be broken down to 77% of the backbone–backbone hydrogen bonds but only 57% of the side chain hydrogen bonds. Those backbone–backbone hydrogen bonds in the crystal structure which are missing in the time-averaged structure are located mainly in the turn and loop regions. In particular, most of the hydrogen bonds in the N-terminal region before helix A have been lost or have changed partners. The irregular surface loop between residues 337 and 347 has also undergone numerous changes in the hydrogen bonding pattern.

We also determined the fraction of time when any particular hydrogen bond was present during the simulation. Not surprisingly, the vast majority of the very stable hydrogen bonds are backbone hydro-

gen bonds between residues in the various secondary structure domains. However, even for this class of hydrogen bonds, there is a wide variation in the frequency of occurrence. For instance, in the first turn of helix F, which shows large structural fluctuations, the expected backbone–backbone hydrogen bonds are present in less than half of the structures. This is in contrast with the remainder of helix F, where the expected hydrogen bonds are present in over 80% of the structures. Likewise for residues Val-119 and Gly-120 in the middle of helix C, the expected hydrogen bonding pattern is present less than half the time, much less than for the other residues in that helix. This is not surprising since as noted above neither residue has helical backbone dihedral angles.

For helices I and L, which are buried in the interior of the protein, most of the expected backbone–backbone hydrogen bonds are present 90% or more of the time. The unusual hydrogen bond between the sidechain hydroxyl of Thr-252 and the carbonyl oxygen of Gly-248 in the middle of helix I is also maintained in 89% of the structures examined while the "correct" backbone–backbone hydrogen bond is present in less than 4% of the simulation. This side chain hydrogen bond between residues that are highly conserved among species has been implicated in maintaining the three-dimensional structure of the oxygen binding pocket of cytochrome P-450_{cam}.[9,12] Its occurrence prevents the normal backbone–backbone hydrogen bonds from forming for these residues and helps to stabilize a distortion away from a helical conformation in the crystal structure. However, it is not only a single backbone hydrogen bond that is missing. The helix defect present in the crystal structure also disrupts the expected hydrogen bonding pattern on both sides of Thr-252. As noted above, this distortion is much smaller in the time-averaged structure than in the starting structure with all residues in this region adopting helical-like conformations. Even though the distortion in the backbone dihedral angles is significantly smaller than in the crystal structure, it is still sufficient to prevent the formation of the normal backbone–backbone hydrogen bonds for these residues. In fact with our criteria for hydrogen bonding, the amide proton of Thr-252 spends over 90% of the time with no hydrogen bonding partner at all, a rather surprising finding for a deeply buried residue. In the time-averaged structure, this amide proton is pointed in the direction of the Gly-248 carbonyl but the average oxygen–amide hydrogen distance is 3.7 vs 1.8 Å for the side chain hydroxyl hydrogen. In part this is due to the presence of water 687, which is wedged in between residues 249 and 253 and prevents the formation of the normal backbone hydrogen bond for these residues. This water, which is part of a postulated solvent access channel, appears to be as important as Thr-252 in preventing the formation of the proper backbone–backbone hydrogen bonds and in stabilizing the kink seen in the crystal structure. Water 687 and the other solvent molecules in this access channel also show low thermal motion and stable hydrogen bonding patterns.

There are also a small number of stable side chain hydrogen bonds that are maintained for much of the trajectory. For instance, Trp-42 and Ser-393 form a stable hydrogen bond present in over 90% of the structures examined which anchors the relative positions of helix A and β-sheet 5. Thr-101 is hydrogen bonded to Tyr-96 throughout the course of the simulation, helping to stabilize the active site geometry. The turn between helices F and G is stabilized by strong hydrogen bonds between Tyr-179 and Ser-190 and between Ser-190 and Gln-183. There is also a side chain–side chain hydrogen bond between Gln-46, at the end of helix A, and Asn-328, a residue in a short 3_{10}-helix just past β-sheet 3, which is present in the vast majority of structures.

On the other hand, some of the side chain hydrogen bonds noted in the crystallographic study turned out to be quite short lived in the simulation. The hydrogen bond between Pro-86 and Gly-298 is present only about a third of the time and the hydrogen bond between Val-345 and Asn-332, which was assumed to stabilize an irregular surface loop, is not found after the initial warmup. In that same surface loop, His-337 spends a much larger fraction of time hydrogen bonded to Asp-339 rather than to Arg-342 as was seen in the crystal structure. It is not surprising that many of the hydrogen bonds in surface turns and loops should be quite short lived since these regions of the protein exhibited the largest deviation away from the crystal coordinates. This high degree of conformational flexibility reflects not only the intrinsic mobility of these regions but also the effect of the minimal amount of explicit solvent present in the simulation, and the absence of crystal packing forces which are not included in this simulation. It should also be noted that a special hydrogen bonding term was not used in the potential function but rather that the formation of hydrogen bonds was determined solely by the electrostatic and van der Waals forces according to the formulation of Lifson and co-workers.[26,27]

Secondary Structure Analysis

In Table II, the average rms deviation over the final 135 psec of the simulation of the backbone atoms of each of the 18 secondary structure elements is listed. The most interesting behavior is exhibited by helix F. The rms deviation of the backbone atoms of helix F is plotted as a function of time in Figure 7. The helix undergoes a distinct conformational change at about 22 psec and again at 34 psec. A more detailed analysis of the motions of helix F indicates that the first turn in helix F was switching between an α-helical conformation and one which

TABLE II. The Average rms Deviation of the Structural Units in Camphor-Bound P-450$_{cam}$

Structural element	rms deviation (Å)
Helix A	0.53
Helix B	0.47
Helix B′	0.46
Helix C	1.13
Helix D	0.57
Helix E	0.67
Helix F	1.09
Helix G	0.91
Helix H	0.52
Helix I	0.84
Helix J	0.54
Helix K	0.44
Helix L	0.47
Sheet 1	0.91
Sheet 2	0.92
Sheet 3	0.54
Sheet 4	0.53
Sheet 5	1.26

was more reminiscent of a 3_{10}-helix. The remainder of helix F stayed in an α-helical conformation throughout the simulation. The relatively large rms deviation calculated for helix C reflects the conformational changes at residues 119 and 120, which, as noted above, do not have typical helical conformations in the X-ray structure.

Both sheets 2 and 5 underwent a fairly large shift during the warmup phase of the simulation but then reached a stable plateau. In the case of β-sheet 2, it appears that a slight widening of the turn between the two strands of the sheet during the warming phase is responsible for the increase in rms deviation. For β-sheet 5, the increase in rms deviation is correlated with changes in the backbone dihedral angles of residues 385 through 388 that result in local distortions but leave the remainder of the sheet region virtually unchanged.

To further probe the motions of the various secondary structure elements, we monitored the angle between the axes of adjacent helices as a function of the time course of the simulation. We defined the axis of a helix to be the eigenvector corresponding to the smallest eigenvalue of the moment of inertia matrix. The moment of inertia matrix for each helix was defined using all of the C-α positions of the helical residues. The resulting matrix was then diagonalized to determine the magnitude and direction of the smallest moment of inertia. From this information, the angle between adjacent helices was determined as a function of time. The average angle for each pair of adjacent helices and the corresponding root mean square fluctuation of each helix–helix angle are listed in Table III. The variations in the interhelical angles represent low-frequency collective motions of the enzyme which may be important for allowing substrate access to the active site. The calculated rms fluctuations range from a high of 6.78° for helices G and H to a low of only 0.33° for the angle between helices B and B′. The observation of a relatively large variation in the angle between the G and H helices along with the mobility previously noted for the F helix suggest that this region contacting the active site may play a crucial role in the access channel. It should be noted that the observed amplitudes and frequencies of these collective motions are likely to be significantly affected by absence of solvent forces.

Analysis of the Atomic Fluctuations

In Figure 8, we have compared the isotropic rms fluctuations of the heavy atoms averaged per amino acid residue calculated from the simulation with the corresponding values calculated using the reported X-ray temperature factors.[9] As has been seen in other molecular dynamics simulations of globular proteins, the theoretically calculated rms fluctuations are generally smaller than those determined from the X-ray temperature factors. The larger experimental values reflect the fact that reported B factors from X-ray structure determinations can include contributions from static disorder, lattice effects, and errors in intensities in addition to the isotropic structural fluctuations they are assumed to measure.[28] Although the experimental fluctuations are greater than the calculated values, there is reasonable qualitative agreement between the two patterns of peaks and valleys. The average rms fluctuation of all the heavy atoms is 0.42 Å, while the average rms fluctuation for just the backbone atoms is 0.37 Å. The values determined from X-ray temperature factors are 0.83 and 0.79 Å, respectively.

The residues with the largest calculated rms fluctuations are in the N-terminal region and β-sheet 4, which contacts the N-terminus in the crystal structure. During the simulation, the first 20 residues have high mobilities which is not unexpected since these residues are on the surface and are not part of any structural unit. In the crystal structure, Leu-22 and His-12 make favorable side chain–side chain contacts with residues in β-sheet 4. These contacts are broken during the simulation because of the high mobility of the N-terminus, resulting in an increased mobility for the residues in β-sheet 4. In contrast with the N-terminus, the C-terminus does not have any residues with particularly large calculated rms fluctuations. The motions are restricted by the strong interactions with the C-terminal end of helix D. Another region displaying a fair amount of mobility is the N-terminal half of helix F. The large calculated fluctuations for these residues are correlated with the structural changes noted above. The residues in the C-terminal half of helix F show

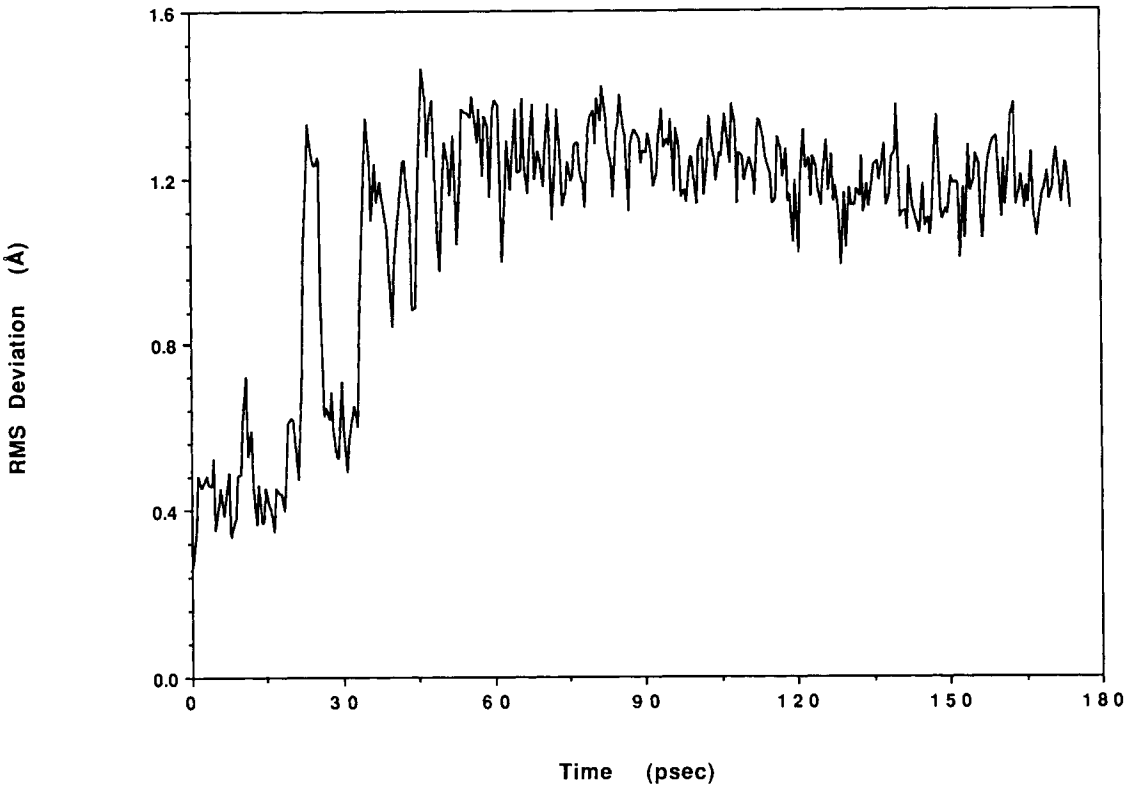

Fig. 7. Rms deviation in Ångstroms of the backbone atoms of helix F plotted as a function of the time course of the simulation.

TABLE III. The Average Angle and rms Fluctuation Between Adjacent Helices

Helices	Average angle (degrees)	rms fluctuation (degrees)
A to B	62.86	2.67
B to B′	1.61	0.33
B′ to C	12.62	3.10
C to D	63.01	2.48
D to E	23.35	2.07
E to F	68.90	1.25
F to G	34.52	1.62
G to H	70.14	6.78
H to I	34.02	4.26
I to J	91.20	0.62
J to K	4.85	0.46
K to L	66.71	2.47

much smaller fluctuations. Conversely, helices I, L, and E along with β-3 all show very small rms fluctuations during the course of the simulation. Helices I and L form a sandwich around the heme moiety at the active site of P-450$_{cam}$. Helix E has extensive contacts with both I and L. Sheet β-3 along with helices I and L are well buried with little solvent exposed surface area. These structural elements appear to form a very stable core region in the enzyme. The general segregation of very mobile residues from residues exhibiting little motion is shown in Figure 9A and B which present a color-coded ribbon structure of cytochrome P-450$_{cam}$. The 10% of the residues with the largest calculated atomic fluctuations are shown in red and the 10% with the smallest fluctuations are shown in blue. Especially in Figure 9B, the very stable core region can be seen shaded in blue surrounded by a ring of much more mobile residues.

In order to separate backbone motions from side chain motions, we have calculated the backbone dihedral angle fluctuations over the final 135 psec of the simulation. In Figure 10, the rms fluctuations in the backbone dihedral angles Φ and Ψ are plotted as a function of residue number. The average rms fluctuation in Φ and Ψ for all residues is 12.9°. In contrast, the average rms fluctuation in the backbone dihedral angle omega is only 7.3°. If only the residues which are part of α-helices are considered, the rms fluctuation in Φ and Ψ is 10.7°. The average for the β-sheet regions is slightly larger at 14.4°, while those residues which are not part of any secondary structure element have an average fluctuation of 15.5°. Of all the secondary structure elements, helix F appears to be the most unusual in its backbone motions. The average rms fluctuations in Φ and Ψ for the N-terminal half of helix F is 13.7°; this is significantly greater than the average for all helical residues and is as large as any observed in the sim-

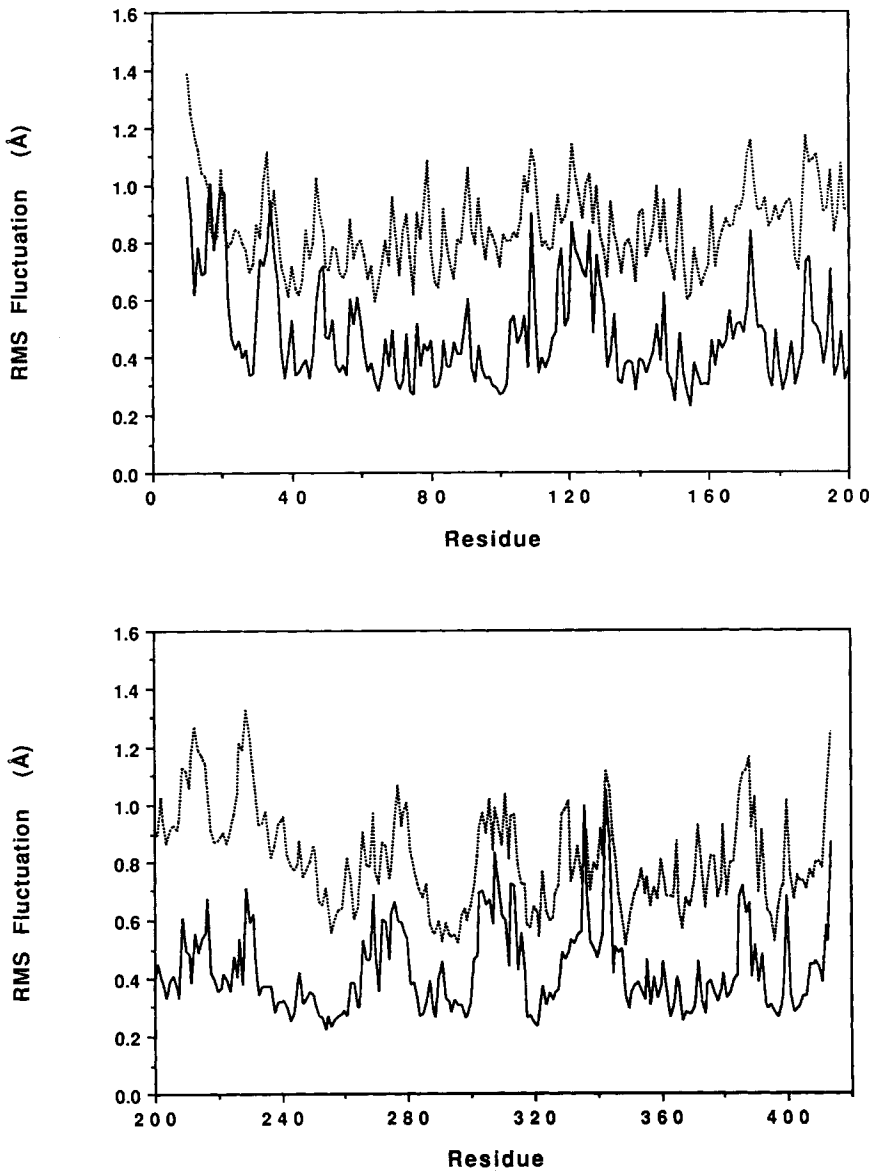

Fig. 8. Rms fluctuations in atomic position of the heavy atoms averaged per residue plotted as a function of residue number. The solid line was calculated from the molecular dynamics trajectory. The dotted line was calculated from the experimental temperature factors.

ulation. These large fluctuations reflect the fact that helix F underwent several conformational switches during the simulation. In contrast the C-terminal half of this helix has an average rms fluctuation of only 9.7°, slightly less than the average for all helical residues. Residues 119 and 120 in helix C and 251 and 252 in helix I also displayed rms fluctuations significantly higher than the average for helical residues. For Val-119 and Gly-120, the dihedral angle fluctuations are large enough to place these residues in the top 10% of backbone dihedral angle fluctuations. These residues were the same ones that showed large changes in dihedral angles between the initial structure and the time-averaged structure. However, the large calculated rms fluctuations for these residues are not directly attributable to the observed conformational changes since the averaging to determine the fluctuations was started after the conformational switches had occurred. In the case of residues 251 and 252, it will be interesting to determine if a simulation of the ternary complex with both camphor and either CO or O_2 results in significantly smaller fluctuations in this region. Most of the other residues with significant fluctuations in backbone dihedral angles are located in the turns between helices or in surface

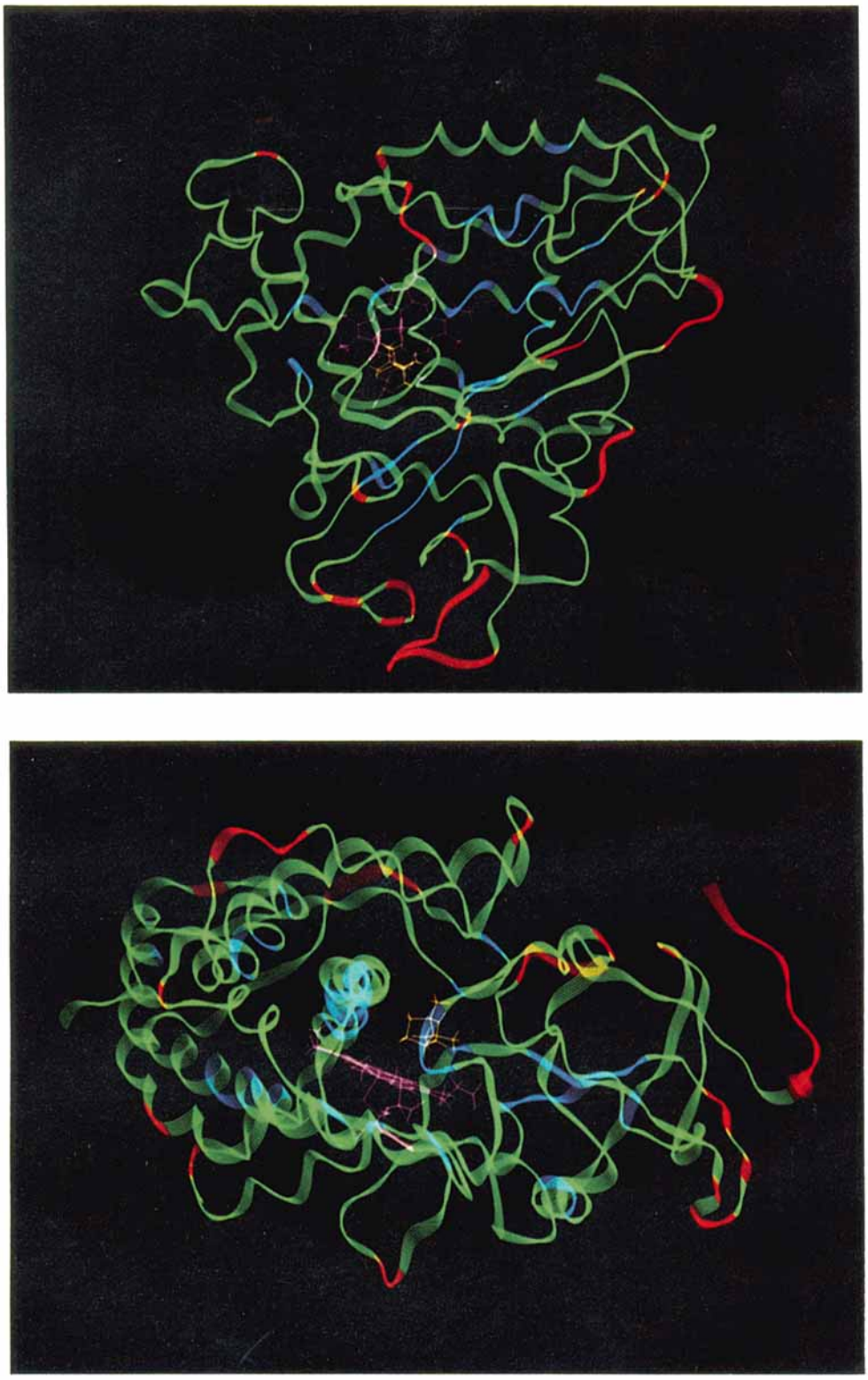

Fig. 9. Two views of a ribbon drawing of cytochrome P-450$_{cam}$ color coded on the basis of rms atomic fluctuations. The 10% of the residues with the largest rms fluctuation are colored red and the 10% with the smallest fluctuations are colored blue. The second view **(Bottom)** is rotated by 90° around the vertical axis from the first **(Top).**

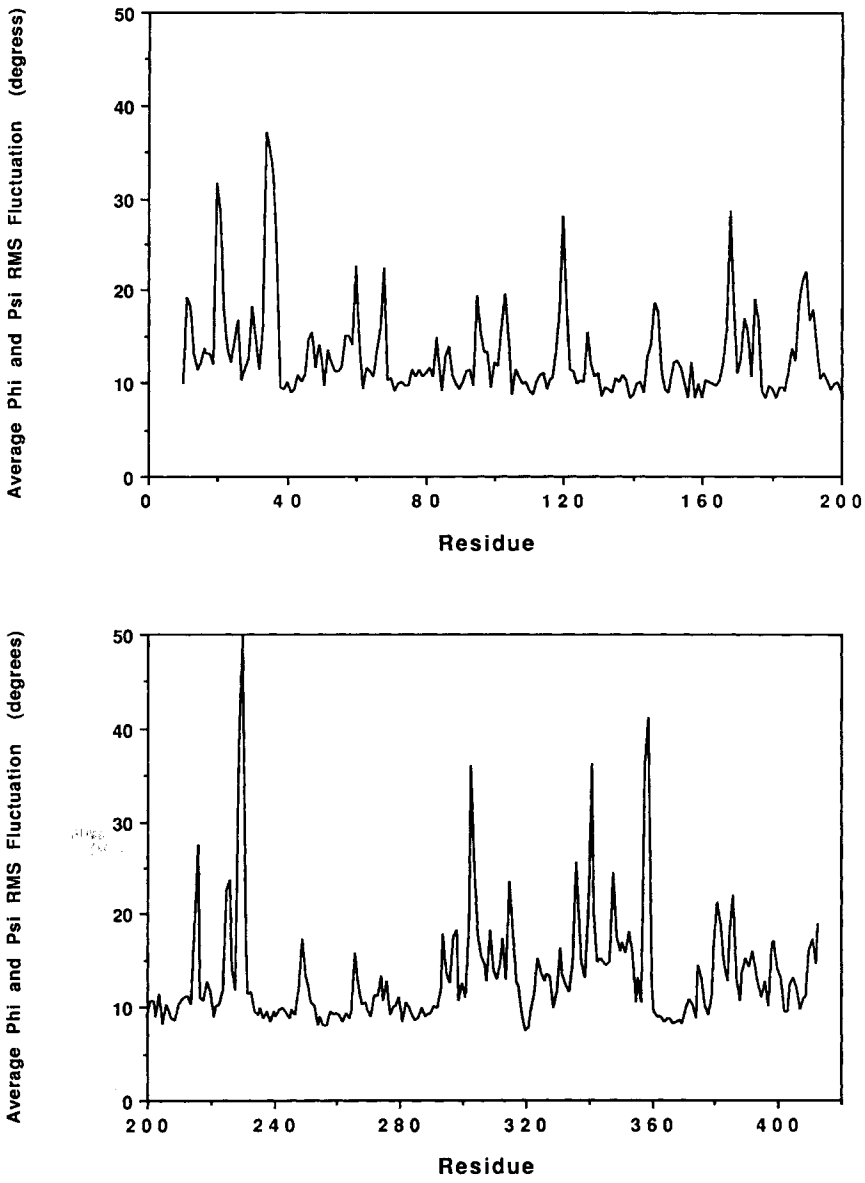

Fig. 10. The average rms fluctuations of the backbone dihedral angles Φ and Ψ.

loops. This can be seen in Figure 11A and B, where a color-coded ribbon diagram of cytochrome P-450_{cam} is presented. Particularly in Figure 11B, the ring of very mobile residues stands in contrast to the core of cold residues near the heme moiety. Although the range of motion seen for the turns near the active site is substantial it is unclear whether these alone will suffice to allow the entry of a molecule as large as camphor (330 $Å^3$).

In Figure 12, the rms fluctuations in the side chain dihedral angle chi 1 for all nonglycine residues are plotted as a function of residue number. The average fluctuation in chi 1 is 12.5°, very similar in magnitude to the averages for the backbone dihedral angles Φ and Ψ. The range of fluctuations is, however, significantly larger. The fluctuations in chi 1 do not correlate nearly as well with secondary structure units as do the fluctuations in Φ and Ψ. Many of the residues with the largest fluctuations are part of secondary structure units. However, the I and L helices and heme binding pocket at the core of the enzyme still show very limited mobilities in chi 1. The strongest correlation, as one might expect, is with side chain, the aromatic residues, whether or not they are in secondary structure elements, are heavily represented in the coldest 10%. Likewise, very small residues such as alanine are well represented in the hottest 10%.

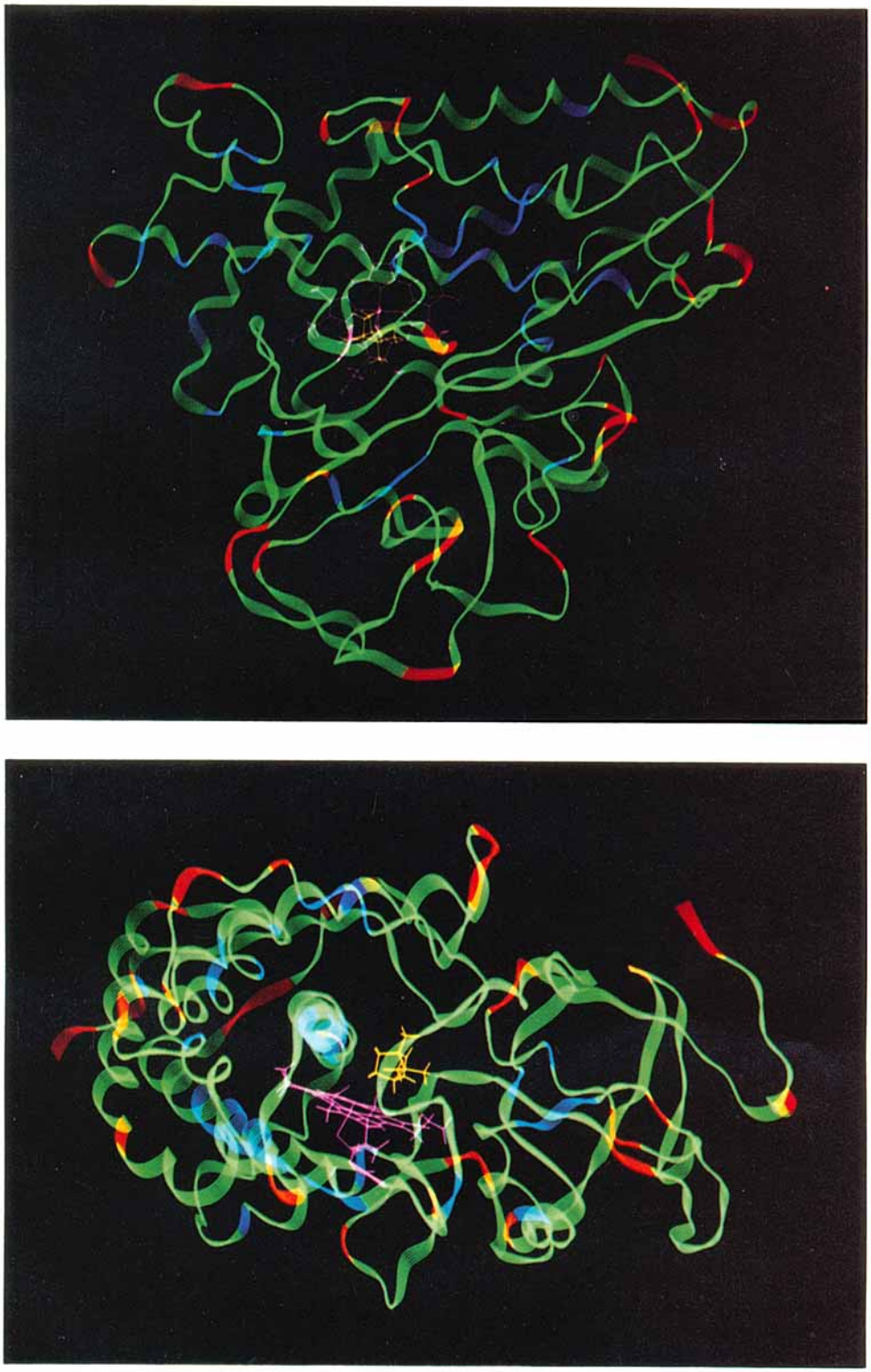

Fig. 11. Two views of a ribbon drawing of cytochrome P-450$_{cam}$ color coded on the basis of rms backbone dihedral angle fluctuations. The 10% of the residues with the largest rms fluctuations are colored red and the 10% with the smallest fluctuations are colored blue. The second view **(bottom)** is rotated by 90° around the vertical axis from the first **(top)**.

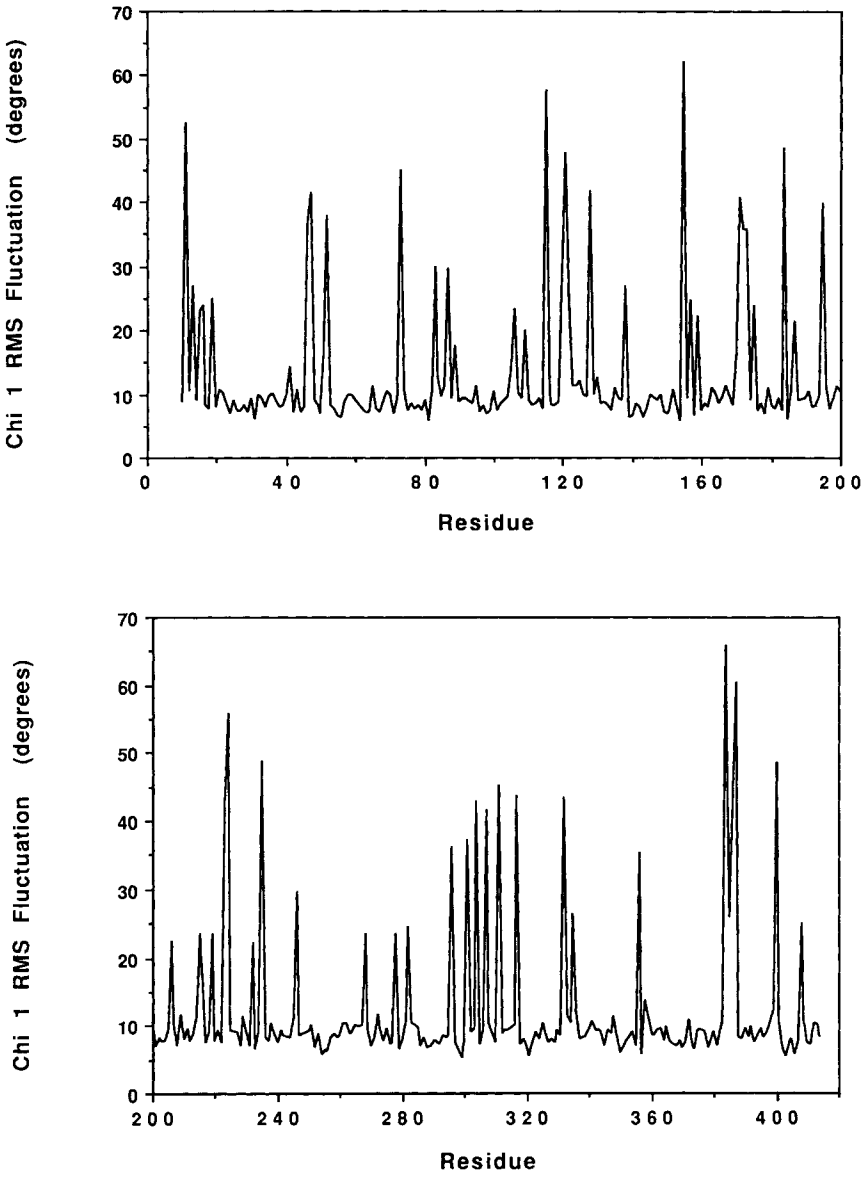

Fig. 12. The rms fluctuations of the side chain dihedral angle chi 1 plotted versus residue number.

CONCLUSIONS

A 175-psec molecular dynamics simulation of cytochrome P-450$_{cam}$ from *Pseudomonas putida* with camphor bound at the active site was performed starting from an energy-minimized structure in order to assess the range of motions accessible to the various domains in the enzyme. We were particularly interested in determining the mobility of those residues likely to be involved in the gate-opening necessary for substrate binding and product release. The time-averaged structure determined from the simulation was quite similar to the beginning X-ray structure. All 13 segments of α-helix and 5 regions of β-sheet structure were preserved in the time-averaged structure, although part of helix F switched between the starting α-helix and a 3_{10}-helix. The regions of largest deviation from the starting structure were generally surface turns and loops, which are the regions most likely to be affected by the approximations used in the simulation, and also by crystal lattice packing forces. The computed atomic fluctuations are in reasonable agreement with those determined from X-ray crystallographic studies and indicate a wide range of mobilities. The secondary structure elements by in large had small calculated

rms fluctuations. Two exceptions to this were in the C and I helices. Residues 119 and 120, which form a kink in the middle of the C helix, and residues 251 and 252, at the oxygen binding site in helix I, both have unusually high mobilities which may have functional implications. In addition, in the I helix, the helix defect at residue 252 disappeared at an early stage of the simulation. This suggests that the conserved threonine at this position is used not to stabilize a structural kink, but rather as a hydrogen bond donor to stabilize a catalytic intermediate. In order to better understand the motions in this functionally important region, we will perform an additional simulation with an axial ligand present in a ternary complex. Several of the turns and surface loops sample large regions of conformational space. In particular, the turns between helices F and G (which sit right above the active site) and between helices G and H show very high flexibility. Whether or not such motions would be sufficient to allow substrate entry and exit is unclear from the present simulation. For any dramatic movement of substrate, such motions would have to be coupled with large movements in amino acid side chains at the active site. At least during the 175 psec simulated, very limited motion was observed in the active site residues. A detailed analysis of the motions of the bound camphor and of the active site residues will be presented elsewhere. Simulations of the substrate-free enzymes are currently underway and hopefully will shed additional light on which residues may be important in allowing substrate access to and from the active site.

ACKNOWLEDGMENTS

The authors would like to thank Gail Sanders and Dr. Michael Bass for providing some of the analysis programs used. We also thank Dr. Bass for helpful discussion and critical reading of this manuscript. Pacific Northwest Laboratory is operated for the U.S. Department of Energy by Battelle Memorial Institute under Contract DE-AC06-76RLO 1830. M. D. Paulsen is supported by the Northwest College and University Association for Science in affiliation with Washington State University under Contract DE-AM06-76-RLO 2225 with the U.S. Department of Energy, Office of Energy Research.

REFERENCES

1. Brooks, C.L., III. Karplus, M., Pettitt, B.M. "Proteins: A Theoretical Perspective of Dynamics, Structure, and Thermodynamics," Adv. In Chem. Phys., 71. New York: Wiley, 1988.
2. McCammon, J.A., Harvey, S.C. "Dynamics of Proteins and Nucleic Acids." Cambridge: Cambridge University Press, 1987.
3. Makinen, M.W., Troyer, J.M., van der Werff, Berendsen, H.J.C., van Gunsteren, W.J. Dynamical structure of carboxypeptidase A. J. Mol. Biol., 207:201–216, 1989.
4. MacKerell, A.D., Nilsson, L., Rigler, R., Heinemann, U., Saenger, W. Molecular dynamics simulations of ribonuclease T_1: Comparison of the free enzyme and the 2′ gmp-enzyme complex. Proteins: Struct. Funct. Genet. 6:20–31, 1989.
5. Brown, F.K., Kollman, P.A. Molecular dynamics simulations of loop closing in the enzyme triose phosphate isomerase. J. Mol. Biol. 198:533–546, 1987.
6. Nebert, D.W., Gonzalez, F.J. P450 genes: Structure, evolution, and regulation. Annu. Rev. Biochem. 56:945–993, 1987.
7. Sligar, S.G., Murray, R.I. Cytochrome P-450cam and other bacterial P-450 enzymes. In: "Cytochrome P450: Structure, Mechanism, and Biochemistry." Ortiz de Montellano, P., ed. New York: Plenum, 1986: 429–503.
8. Poulos, T.L., Finzel. B.C., Howard, A.J. Crystal structure of substrate-free pseudomonas putida cytochrome P-450. Biochemistry 25:5314–5322, 1986.
9. Poulos, T.L., Finzel, B.C., Howard, A.J. High-resolution crystal structure of cytochrome P-450cam. J. Mol. Biol. 195:687–700, 1987.
10. Poulos, T.L., Howard, A.J. Crystal structures of metyrapone- and phenylimidazole-inhibited complexes of cytochrome P-450cam. Biochemistry 26:8165–8174, 1987.
11. Raag, R., Poulos, T.L. The structural basis for substrate-induced changes in redox potental and spin equilibrium in cytochrome P-450cam. Biochemistry 28:917–922, 1989.
12. Raag, R., Poulos, T.L. Crystal structure of the carbon monoxide substrate-cytochrome P-450cam ternary complex. Biochemistry 28:7586–7592, 1989.
13. Bernstein, F.C., Koetzle, T.F., Williams, G.J.B., Meyer, E.F., Jr., Brice, M.D., Rodgers, J.R., Kennard, O., Shimanouchi, T., Tasumi, M. The protein data bank: A computer-based archival file for macromolecular structures. J. Mol. Biol. 112:535–542, 1977.
14. Ornstein, R.L. Using molecular dynamics simulations on crambin to evaluate the suitability of different continuum dielectric and hydrogen atom models for protein simulations. J. Biomol. Struct. Dyn. 7:1019–1041, 1990.
15. Hagler, A.T. Theoretical simulation of conformation, energetics, and dynamics of peptides In: "Conformation in Biology and Drug Design, The Peptides," Vol. 7. Hruby, V.J., Meienhofer, J., eds. New York: Academic Press, 1985: 213–299.
16. Dauber-Osguthorpe, P., Roberts, V.A., Osguthorpe, D.J., Wolff, J., Genest, M., Hagler, A.T. Structrure and energetics of ligand binding to proteins: Escherichia coli dihydrofolate reductase-trimethoprim, a drug-receptor system. Proteins: Struct. Funct. Genet. 4:31–47, 1988.
17. Giammona, D.A. Ph.D. Dissertation, University of California Davis, 1986.
18. Berendsen, H.J.C., Postma, J.P.M., van Gunsteren, W.F., DiNola, A., Haak, J.R. Molecular dynamics with coupling to an external bath. J. Chem. Phys. 81:3684–3690, 1984.
19. Post, C.B., Brooks, B.R., Karplus, M., Dobson, C.M., Artymiuk, P.J., Cheetham, J.C., Phillips, D.C. Molecular dynamics simulations of native and substrate-bound lysozyme. J. Mol. Biol. 190:455–479, 1986.
20. Lewis, B.A., Sligar, S.G. Structural studies of cytochrome P-450 using small angle X-ray scattering. J. Biol. Chem. 258:3599–3601, 1983.
21. van Gunsteren, W.F., Berendsen, H.J.C., Hermans, J., Hol, W.G.J., Postma, J.P.M. Computer simulation of the dynamics of hydrated protein crystals and its comparison with X-ray data. Proc. Natl. Acad. Sci. U.S.A. 80:4315–4319, 1983.
22. Åqvist, J., van Gunsteren, W.F., Leijonmarck, M., Tapia, O. A molecular dynamics study of the C-terminal fragment of the L7/L12 ribosomal protein: Secondary structure motion in a 150 ps trajectory. J. Mol. Biol. 183:461–477, 1985.
23. McCammon, J.A., Gelin, B.R., Karplus, M. Dynamics of folded proteins. Nature (London) 267:585–590, 1977.
24. Imai, Y., Shimada, H., Watanabe, Y., Matsushima-Hibiya, Y., Makino, R., Koga, H., Horiuchi, T., Ishimura, Y. Uncoupling of the cytochrome P-450cam monooxygenase reaction by a single mutation, threonine-252 to alanine or valine: A possible role of the hydroxy amino acid in oxygen activation. Proc. Natl. Acad. Sci. U.S.A. 86:7823–7827, 1989.
25. Martinis, S.A., Atkins, W.M., Stayton, P.S., Sligar, S.G. A conserved residue of cytochrome P-450 is involved in oxygen activation. J. Am. Chem. Soc. 111:9252–9253, 1989.
26. Hagler, A.T., Huler, E., Lifson, S. Energy functions for

peptides and proteins. I. Derivation of a consistent force field including the hydrogen bond from amide crystals. J. Am. Chem. Soc. 96:5319–5335, 1974.
27. Hagler, A.T., Lifson, S., Duaber, P. Consistent force field studies of intermolecular forces in hydrogen bonded crystals. II. A benchmark for the objective comparison of alternative force fields. J. Am. Chem. Soc. 101:5122–5130, 1979.
28. McCammon, J.A., Karplus, M. The dynamic picture of protein structure. Acc. Chem. Res. 16:187–193, 1983.